

Structural and physical properties of the misfit intercalation compounds Hg_xTaS_2 ($x = 0.58, 1.19, \text{ and } 1.3$)

P. Ganal, P. Moreau, G. Ouvrard, W. Olberding,* and T. Butz†

Institut des Matériaux de Nantes, 2, rue de la Houssinière, 44072 Nantes, France

(Received 17 April 1995)

Time-differential perturbed angular correlation (TDPAC) and x-ray powder diffraction (XPD) have been used to investigate the complex physical and structural properties of mercury intercalation compounds derived from $1T\text{-TaS}_2$ and $2H\text{-TaS}_2$, respectively. *In situ* TDPAC studies of the ^{181}Ta nuclear quadrupole interaction during Hg intercalation and thermal deintercalation proved the complete reversibility of the intercalation process and revealed the formation of three distinct phases ($\alpha\text{-Hg}_{1.19}\text{TaS}_2$, $\beta\text{-Hg}_{1.3}\text{TaS}_2$, and a disordered second-stage phase $\text{Hg}_{0.58}\text{TaS}_2$ derived from $\alpha\text{-Hg}_{1.19}\text{TaS}_2$). The stage-1 compounds $\alpha\text{-Hg}_{1.19}\text{TaS}_2$ and $\beta\text{-Hg}_{1.3}\text{TaS}_2$ are characterized by two different structural arrangements of the intercalated Hg that bear a strong resemblance to those realized in solid-state phases of $\beta\text{-Hg}$ and $\alpha\text{-Hg}$, respectively. $\alpha\text{-Hg}_{1.19}\text{TaS}_2$ adopts an unusual (3+1)-dimensional composite crystal structure which can be described as two interpenetrating sublattices formed by the TaS_2 host and the Hg guest. These *C*-face-centered orthorhombic sublattices share common *a* and *c* axes but are incommensurate along the *b* axis [$a = 5.765(1) \text{ \AA}$, $b = 3.309(1) \text{ \AA}$, $c = 17.842(1) \text{ \AA}$, and $b_{\text{Hg}} = 2.782(1) \text{ \AA}$]. The in-plane Hg-Hg distances of 2.782 and 3.201 \AA indicate a chainlike Hg arrangement similar to that found in $\text{Hg}_{1.24}\text{TiS}_2$. In the case of $\beta\text{-Hg}_{1.3}\text{TaS}_2$ the Hg arrangement is such that the TaS_2 host lattice ($a = 3.318 \text{ \AA}$) can be considered as a 2×2 superstructure formed upon hexagonal close-packed Hg layers ($a_{\text{Hg}} = 2.902 \text{ \AA}$). Hg intercalation into $1T\text{-TaS}_2$ requires an elevated reaction temperature of 423 K, whereas $2H\text{-TaS}_2$ intercalates Hg already at ambient temperature. Both the TDPAC and x-ray-diffraction data indicate that in the case of $1T\text{-TaS}_2$ the Hg intercalation process is accompanied by an irreversible change of the TaS_2 host layers from octahedral to a trigonal-prismatic arrangement.

I. INTRODUCTION

Layered transition-metal dichalcogenides MX_2 are well known for their ability to form intercalation compounds accepting a large variety of guest species (both atoms and molecules).¹⁻³ Structurally, they are composed of XM_2 layers with the transition metals atoms *M* sandwiched between two hexagonal close-packed chalcogen sheets *X*. There are two principal types of MX_2 lamellas depending on the coordination of the transition-metal atoms, with respect to their chalcogen surrounding (either octahedral or trigonal-prismatic).² From these two basic constituents, various polymorphs can be derived from different stacking modes, but, in general, only one of these modifications is thermodynamically stable. However, in many cases such as TaS_2 or NbS_2 , the high-temperature modifications can be retained by rapid quenching.^{2,4,5}

Characteristic for all transition metal dichalcogenides (TMD's) of the layered type is the large anisotropy in their chemical bonds. Within the MX_2 layers, covalent metal-chalcogen bonds are formed, whereas the lamellas themselves are kept together by weak forces of van der Waals (vdW) type. As a consequence intercalation is, in general, accompanied by a lattice expansion perpendicular to the layers, but has little or no effect on the structure of the MX_2 lamellas. In many cases, reversible shear transformations take place upon intercalation, which alter the stacking sequence and thus allow the guest to reside on specific lattice sites. However, it has been shown

that in some rare cases, e.g., Li_xMoS_2 ($2H$) and Li_xTaS_2 ($1T$), intercalation can even induce a change of the transition-metal coordination within the MX_2 layers.⁶⁻⁸

One of the most intensely investigated classes of guests that form TMD intercalation compounds (TMDIC's) are elemental metals.^{1,2} These intercalants are generally believed to form ionic guests and occupy discrete lattice sites in the vdW gap. However, mercury-intercalated TMD's exhibit some properties that cannot be explained within this general description.⁹⁻¹³ These properties include the ability to intercalate "superstoichiometric" levels of Hg in monolayer form, weak electronic guest-host interactions that appear to be primarily covalent in character, and the indication of unusually complex structures based on x-ray powder diffraction (XPD). Although the Hg-TMDIC's Hg_xNbS_2 and Hg_xTaS_2 were first prepared in the early 1970s,^{14,15} it was only recently that with $\text{Hg}_{1.24}\text{TiS}_2$ the average structure of the first Hg-TMDIC has been resolved.^{16,17}

Hg intercalation into TiS_2 results in an unusual (3+1)-dimensional composite crystal structure, which can alternatively be described by two interpenetrating monoclinic TiS_2 and Hg sublattices. These sublattices share two commensurate axes (*a* and *c*), but are incommensurate along their common *b* axis. The Hg sublattice is made up of infinite one-dimensional Hg metal chains, which are embedded in nearly trigonal-prismatic sulfur channels created by the restacked TiS_2 host layers. Similar chain-

like arrangements of metallic Hg have been reported for the $\text{Hg}_{3-8}\text{MF}_6$ ($M = \text{As, Sb, Nb, Ta}$) family of compounds¹⁸⁻²² and $\beta\text{-Hg}$.²³

In this work, we investigated the intercalation of mercury into $2H\text{-TaS}_2$ and $1T\text{-TaS}_2$, respectively. In order to explore the complex structural properties of these materials, as well as the intercalation process itself, we have combined the complementary techniques of x-ray diffraction (XRD) and time-differential perturbed angular correlation (TDPAC). The latter technique allows an *in situ* investigation of the intercalation process and thus a direct reaction control. The first part of this paper is devoted to the presentation of the TDPAC results. Here, we will introduce the different phases that are formed upon Hg intercalation into TaS_2 , describe their thermal stability, and report on the thermal evolution of their nuclear quadrupole interaction (NQI) signals. Subsequently, we will discuss the structural aspects that can be deduced from the XRD powder data and finally address typical questions such as the ideal composition of these phases, the Hg arrangements realized in the vdW gap, the degree of charge transfer, and their guest host as well as guest-guest interactions.

II. EXPERIMENTAL

A. TDPAC theory, data reduction and data analysis

$\gamma\text{-}\gamma$ TDPAC requires a nucleus in an excited state (here, ^{181}Ta , $I = +\frac{1}{2}$), which decays via the successive emission of two γ quanta. The topmost excited state of ^{181}Ta is, in our case, fed via β^- decay from the neighboring ^{181}Hf isotope ($T_{1/2} = 42.4d$). Its decay spin sequence is $\frac{1}{2} \rightarrow \frac{3}{2} \rightarrow \frac{7}{2}$ with a pure $E2$ and a mixed $M1/E2$ transition, respectively.²⁴ A time resolved coincidence measurement of both γ quanta yields an exponentially decreasing countrate with the lifetime τ_n of the intermediate state (here, $\tau_n = 15.3$ ns).

Due to angular momentum conservation, there is a correlation between the orientation of the nuclear spin and the spatial emission probability for each γ quantum. Consequently, the emission of γ_2 depends on the emission direction \vec{k}_1 of γ_1 .²⁵

$$\begin{aligned} \mathcal{W}(\vec{k}_1, \vec{k}_2, t) \propto & \sum_{k_1, k_2, N_1, N_2} \frac{1}{\sqrt{(2k_1+1)(2k_2+1)}} \\ & \times A_{k_1 k_2} Y_{k_1}^{N_1*}(\vartheta_1, \varphi_1) Y_{k_2}^{N_2}(\vartheta_2, \varphi_2). \end{aligned} \quad (1)$$

Here, $Y_{k_i}^{N_i}$ are spherical harmonics and the $A_{k_1 k_2}$ denote the anisotropy coefficients of the $\gamma\text{-}\gamma$ cascade (here, $A_{22} = -0.268$, $A_{24} = -0.062$, $A_{42} = -0.318$, and $A_{44} = -0.072$).²⁶ Implied by Eq. (1) is the assumption that the spin orientation, which the nucleus adopts after the emission of γ_1 , is preserved until the emission of γ_2 takes place. However, extra nuclear fields, which act on the nucleus while it is in the intermediate state, will change the spin orientation and thus introduce a time-dependent perturbation $G_{k_1 k_2}^{N_1 N_2}(t)$.

$$\begin{aligned} \mathcal{W}(\vec{k}_1, \vec{k}_2, t) \propto & \sum_{k_1, k_2, N_1, N_2} \frac{1}{\sqrt{(2k_1+1)(2k_2+1)}} \\ & \times A_{k_1 k_2} G_{k_1 k_2}^{N_1 N_2}(t) Y_{k_1}^{N_1*} \\ & \times (\vartheta_1, \varphi_1) Y_{k_2}^{N_2}(\vartheta_2, \varphi_2). \end{aligned} \quad (2)$$

In the case of nuclear quadrupole interactions or, more specifically, the interaction of a time-independent electric-field gradient (EFG) with the nuclear quadrupole moment Q of a spin $\frac{5}{2}$ state (here $Q_{\frac{5}{2}} = 2.35b$), the perturbation functions $G_{k_1 k_2}^{N_1 N_2}(t)$ can be expressed in the form²⁷

$$G_{k_1 k_2}^{N_1 N_2}(t) = \sum_{i=0}^3 f_{i, k_1 k_2}^{N_1 N_2}(\eta) \cos \omega_i t \quad (\omega_0 = 0). \quad (3)$$

The precession frequencies ω_i are proportional to the energy splitting of the spin $\frac{5}{2}$ levels due to the NQI,

$$\begin{aligned} \hbar \omega_1 &= E_{\pm \frac{3}{2}} - E_{\pm \frac{1}{2}}, \\ \hbar \omega_2 &= E_{\pm \frac{5}{2}} - E_{\pm \frac{3}{2}}, \\ \hbar \omega_3 &= E_{\pm \frac{5}{2}} - E_{\pm \frac{1}{2}} = \hbar \omega_1 + \hbar \omega_2, \end{aligned} \quad (4)$$

and, in the principal coordinate system, the asymmetry parameter η is related to the tensor components V_{ij} of the EFG by

$$\eta = (V_{xx} - V_{yy}) / V_{zz}. \quad (5)$$

After the insertion of Eq. (3) into Eq. (2) and a resummation of terms the angular correlation function can be written in the comparatively simple form:

$$\begin{aligned} \mathcal{W}(\vec{k}_1, \vec{k}_2, t) \sim & e^{-t/\tau_a} \left[1 + \sum_{i=0}^3 a_i(\vec{k}_1, \vec{k}_2, \eta) \cos \omega_i t \right] \\ & (\omega_0 = 0). \end{aligned} \quad (6)$$

Note that the intensity coefficients a_i are entirely determined by the nuclear parameters of the $\gamma\text{-}\gamma$ cascade, the asymmetry parameter η , and the geometry of the coincidence measurement. Although they can be calculated theoretically, it is for many solid state applications sufficient to treat them as free parameters which can be fitted to the experimental data.

If not stated otherwise, we worked with a conventional four-detector TDPAC setup equipped with BaF_2 γ detectors. Eight out of twelve possible coincidences [of the type Eq. (6)] at angles $\theta = 90^\circ$ and 180° between the γ detectors were recorded simultaneously. In order to reduce the data, we formed the ratio

$$R(t) = 2 \frac{\overline{W}(180^\circ, t) - \overline{W}(90^\circ, t)}{\overline{W}(180^\circ, t) + 2\overline{W}(90^\circ, t)}, \quad (7)$$

where $\overline{W}(\theta, t)$ denotes the fourth root of the product of four equivalent spectra, already corrected for their chance coincidence background. This kind of data reduction has the advantage that the detector efficiencies, as well as the effects of a possible source miscentering, are canceled to

first order. The data analysis was completed by a fast Fourier transform (cosine transform) and a nonlinear least-squares-fit analysis based on Eq. (6).²⁸

As long as all Ta atoms are subjected to the same EFG, the Fourier-transformed perturbation function will show three peaks at the precession frequencies ω_i (apart from a peak at $\omega=0$). All peaks will have instrumental linewidth (roughly 75 Mrad/s) which is determined by the finite time window in which data are recorded (here, typically 80 ns). Slight variations of the EFG around its mean value will give rise to an excess linewidth, which we described approximately by a Gaussian frequency distribution. Time-dependent fluctuations of the EFG (e.g., caused by intercalate hopping) will also contribute to the excess linewidth. However, this contribution vanishes if the fluctuations are fast enough (motional narrowing). For more details concerning TDPAC and practical application, we refer to the following papers and the references given therein.^{27,29,30}

B. X-ray diffraction

XPD measurements were performed in Debye-Scherrer geometry on an INEL powder diffractometer equipped with a position sensitive curved CPS120 detector and a bent quartz monochromator. The incident x-ray beam consisted of the monochromated CuK-L_3 radiation ($\lambda = 1.540598 \text{ \AA}$) generated by a sealed copper x-ray tube operated at 40 kV and 30 mA. Calibrated with cubic $\text{Na}_2\text{Ca}_3\text{Al}_2\text{F}_{14}$ as external calibration standard, the diffractometer offered an overall accuracy of $\delta_{2\theta} \sim 0.009^\circ$. In order to minimize the problems related to preferred orientation and a high absorption coefficient, we coated the external part of small Lindemann capillaries ($\varnothing = 0.01 \text{ mm}$) with crystalline powders of less than $50 \mu\text{m}$ (sieve fraction). Further information about the diffractometer and the data processing are given elsewhere.^{31,32}

C. Sample preparation

$1T\text{-TaS}_2$ and $2H\text{-TaS}_2$ were prepared by an iodine vapor transport reaction from 99.95% pure Ta foils of $15 \mu\text{m}$ thickness and 99.95% pure sulfur in slight excess ($\sim 3\%$). The sealed quartz ampoules were first heated up to 1193 K with a temperature gradient over the ampoule of about 100 K. After four days, the ampoules were either quenched into water (to retain the $1T$ modification) or were subsequently annealed at 1073, 873, and 773 K for 24 h at a time. For the TDPAC measurements, the samples were doped with 200-ppm neutron irradiated hafnium metal (in order to produce ^{181}Hf) during crystal growth. The quality of our $2H\text{-TaS}_2$ and $1T\text{-TaS}_2$ batches was checked by x-ray diffraction and by their TDPAC spectra. A discrete frequency of $\omega = 818 \text{ Mrad/s}$ with instrumental linewidth and a characteristic frequency distribution due to the charge-density wave (CDW) present in $1T\text{-TaS}_2$ at 300 K was considered a stringent criterion for high-quality $2H\text{-TaS}_2$ and $1T\text{-TaS}_2$, respectively.

III. RESULTS

A. Mercury intercalation into $2H\text{-TaS}_2$

1. Room-temperature intercalation

Using the "Munich TDPAC Camera,"³³ we monitored the mercuration of large $2H\text{-TaS}_2$ crystals ($\varnothing \sim 5 \text{ mm}$) *in situ*. All manipulations, such as the selection of the single crystals or the addition of the constituents, have been carried out in air. A stacked plot of Fourier-transformed TDPAC spectra recorded during intercalation is shown in Fig. 1(a).

The amplitude of the NQI signal of pristine $2H\text{-TaS}_2$ ($\omega_1 \sim 818 \text{ Mrad/s}$ plus its harmonics ω_2 and ω_3) decreased steadily after the addition of Hg, while at the same time, two new sets of frequencies appeared at $\omega'_1 \sim 699 \text{ Mrad/s}$ and $\omega''_1 \sim 620 \text{ Mrad/s}$ (plus their har-

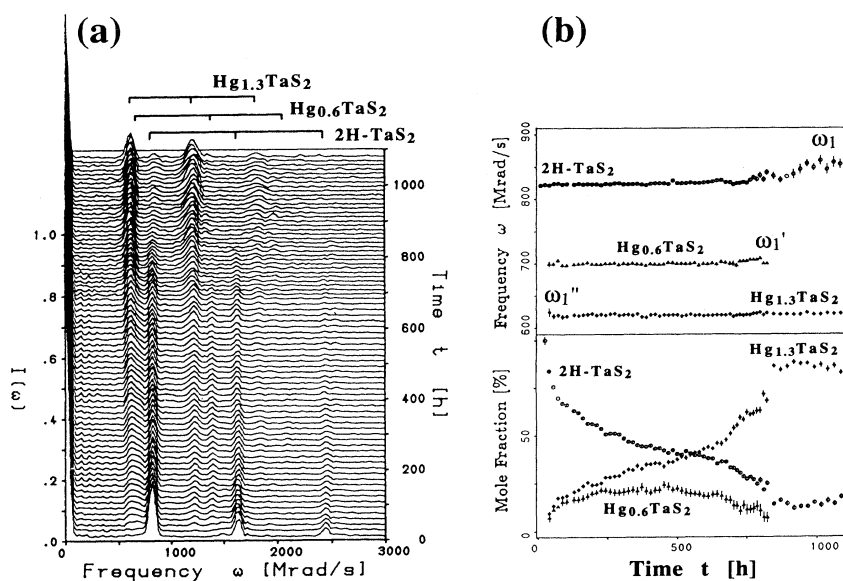


FIG. 1. (a) Stacked plot of Fourier-transformed TDPAC spectra recorded during room-temperature intercalation of Hg into $2H\text{-TaS}_2$. (b) Precession frequencies and mole fractions as obtained by a least-squares-fit analysis. Upon Hg intercalation, two precession frequencies (plus harmonics) attributed to second or random stage compound and $\beta\text{-Hg}_x\text{TaS}_2$ appeared.

monics). The intensity of the frequency ω_1'' increased continuously as the reaction developed, whereas the component ω_1 evolved and disappeared after some time. According to the different time evolution, we attribute the frequencies ω_1' and ω_1'' to an intermediate phase and the final product (β phase), respectively.

The results of a nonlinear least-squares data analysis assuming three different Ta sites with nearly axially symmetric EFG ($\eta \sim 0$) are illustrated in Fig. 1(b) and summarized in Table I. Note, that the preexposure of the $2H\text{-TaS}_2$ crystals to air resulted in a considerable deterioration of the mercuration process. Without exposure to air and in good contact with the liquid Hg, the intercalation reaction is usually finished within several minutes. The precession frequencies of the intermediate phase ω_1' and of the final product ω_1'' were found to be constant throughout the entire reaction [Fig. 1(b), top]. Only for the component ω_1 attributed to pristine $2H\text{-TaS}_2$, could a slight increase in frequency be detected towards the end of the reaction (up to $\omega_1 \sim 860$ Mrad/s). The linewidth of the components ω_1 and ω_1' remained instrumental, whereas the NQI signal of the final product ω_1'' broadened towards the end of the reaction. At the same time, we observed a change of the crystal color from black metallic to a copperlike reddish. Correlated with this color change and the line broadening, the NQI signal of the final product (ω_1'') exhibited a slight but significant deviation from axial symmetry [$\eta \sim 0.11(1)$]. For both the pristine $2H\text{-TaS}_2$ (ω_1) and the intermediate phase (ω_1'), no deviation from axial symmetry could be detected.

The kinetics of the intercalation reaction was largely dominated by nucleation and contact problems. E.g., a rigorous mechanical stirring of the sample after about 800 h resulted in a sudden increase of the mole fraction of the final product [Fig. 1(b), bottom], whereas the mole fractions of the pristine $2H\text{-TaS}_2$ and the intermediate phase decreased or dropped beyond our instrumental resolution.

In order to determine the Hg uptakes of the different phases, as well as to investigate the changes exhibited by the frequency component ω_1'' , we prepared several samples with defined formal Hg contents ($y = 0.34$, $y = 0.93$, and $y > 1.3$). The samples had been annealed at 423 K

for several days prior to the TDPAC measurements in order to ensure complete intercalation. Figure 2 presents some typical TDPAC spectra and their Fourier transforms obtained at 423 and 77 K, respectively.

Samples prepared with Hg excess ($y > 1.3$) exhibited a single Ta site with a fundamental frequency at $\omega_1'' \sim 620$ Mrad/s and its harmonics which broadened considerably at low temperatures (Fig. 2, bottom). Judging from reddish crystal color and the NQI signal, the corresponding homogeneous intercalation product can be easily identified as the above-mentioned final product (β phase).

Formal Hg uptakes around $y \sim 1.0$ resulted in a black-metallic product whose TDPAC spectra (Fig. 2, middle right) also exhibited a dominant fundamental frequency at $\omega_1'' \sim 620$ Mrad/s. In addition, some smaller contributions appeared at the precession frequencies $\omega_1' \sim 699$ Mrad/s and $\omega_1 \sim 818$ Mrad/s, which are characteristic for the intermediate phase and pristine $2H\text{-TaS}_2$. However, in clear contrast to the NQI signal for the β phase, the dominant component with a fundamental frequency ω_1'' exhibited neither a significant line broadening at 77 K nor could we detect any deviation from axial symmetry ($\eta = 0$) (Fig. 2, middle left). We are hence led to the conclusion that there is a second phase somewhat lower in Hg content (α phase), whose NQI signal coincides with that of the final product (β phase). Although the existence of this phase is difficult to prove by TDPAC, it can be easily distinguished from the β phase by the black metallic crystal color, and as we shall discuss later, by diffraction techniques.

Samples prepared with low formal Hg uptakes were usually a phase mixture consisting of pristine $2H\text{-TaS}_2$ ($\omega_1 \sim 818$ Mrad/s), the intermediate phase ($\omega_1' \sim 690$ Mrad/s), and a small contribution of the α phase (Fig. 2, top right). The NQI signal of the intermediate phase (ω_1') remained instrumental down to 77 K and did not exhibit any deviation from axial symmetry. Based on the formal compositions y_i , the mole fractions α_k determined by the TDPAC technique, and the linear relation^{30,34}

$$\alpha_1 x_1 + \alpha_2 x_2 = y_i \quad (8)$$

TABLE I. Hyperfine parameters of $1T\text{-TaS}_2$, $2H\text{-TaS}_2$, and their mercury intercalates. The hyperfine parameters listed comprise for each compound and Ta-site the precession frequency ω , the asymmetry parameter η , the excess linewidth δ describing the broadening of the NQI signal with respect to the linewidth of the TDPAC instrument, the linear temperature variation coefficient $d\omega/dT$ of the precession frequency, and, in the case of the Hg intercalation compounds, the charge transfer n estimated via the empirical relation stated in Eq. (9) in the text.

Compound	ω (Mrad/s)	η	δ (%)	$d\omega/dT$ (Mrad/s/K)}	n (e^-/Ta)
$1T\text{-TaS}_2$	719(2)	0.18(1)	5.2(3)	-0.31(2)	
	820(2)	0.19(1)	2.1(1)	-0.47(5)	
$\beta\text{-Hg}_{1.3}\text{TaS}_2$ (1T)	617(1)	0.08(2)	4.0(1)	-0.07(1)	0.32
$2H\text{-TaS}_2$	818(1)	0.0	0.0	-0.15(1)	
$\text{Hg}_{0.58}\text{TaS}_2$	701(1)	0.0	0.0	-0.11(1)	0.18
$\alpha\text{-Hg}_{1.19}\text{TaS}_2$ (2H)	615(2)	0.0	0.0	-0.08(1)	0.32
$\beta\text{-Hg}_{1.3}\text{TaS}_2$ (2H)	620(2)	0.11(1)	3.5(3)	-0.09(2)	0.32

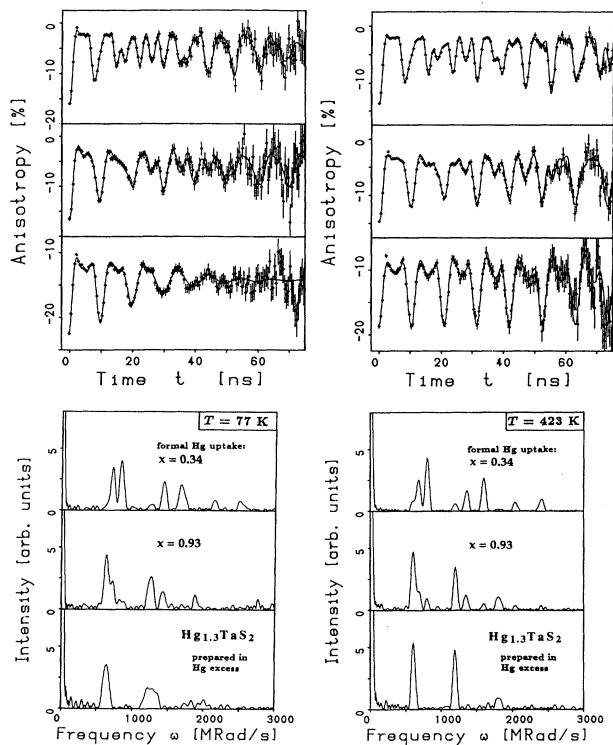


FIG. 2. TDPAC spectra of partly and fully intercalated $2H\text{-TaS}_2$ at $T=77\text{ K}$ (left) and $T=423\text{ K}$ (right), respectively. For the preparation, formal Hg uptakes of $x=0.34$, $x=0.93$, and $x > 1.3$ have been used.

specific Hg uptakes of $x_1=0.57(4)$ and of $x_2=1.19(4)$ can be estimated for the intermediate phase and for the α phase, respectively. These estimates are in good agreement with thermogravimetric analysis (TGA) studies,³⁵ which revealed reproducible decomposition steps at $x_1=0.58(2)$ and $x_2=1.12(2)$. Since the Hg uptake of the intermediate phase is about half as large as that of the α phase, and since the temperature evolution of the NQI signal is quite similar for both phases, one may consider

the intermediate phase as a second-stage compound derived from the α phase. Further evidence supporting this idea will be discussed later on.

2. Thermal deintercalation of mercury

The stability of the different Hg-intercalate phases depends strongly on the temperature but also on the temperature gradient within the sealed glass ampoule. For small temperature gradients and temperatures up to 393 K, $\beta\text{-Hg}_x\text{TaS}_2$ remained stable as proved by XPD. In those cases only, the excess Hg was transported towards the colder end of the ampoule. The use of larger temperature gradients or higher temperatures usually resulted in a phase mixture consisting of $\alpha\text{-Hg}_x\text{TaS}_2$, the second-stage phase, and residual $2H\text{-TaS}_2$. In order to illustrate this in a more quantitative way, a $\beta\text{-Hg}_x\text{TaS}_2$ sample was filled in one end of a U -shaped silica tube and placed inside a small vertical oven which was located between the γ detectors of a conventional four-detector TDPAC setup. The other end of the U -shaped tube was placed in a dry ice/methanol bath ($T=194.5\text{ K}$) in order to keep the Hg vapor pressure low. The temperature inside the heater was controlled by a PtRhPt thermocouple. A stacked plot of Fourier transformed TDPAC spectra recorded during the experiment is shown in Fig. 3(a).

At room temperature, no change of the TDPAC signal could be detected even after a period of two days [Fig. 3(a), first spectrum]. Upon heating the sample to 348 K, a decrease of the excess linewidth of the NQI signal ($\omega_1'' \sim 618\text{ Mrad/s}$) by about 50% is observed [Fig. 3(a), second spectrum]. In addition, a tiny shoulder appeared at $\omega_1' \sim 684\text{ Mrad/s}$ (second-stage phase). This as well as the decrease in linewidth clearly indicated the onset of the Hg deintercalation. Raising the temperature to 398 K accelerated the deintercalation process considerably and a third frequency component at $\omega_1 \sim 804\text{ Mrad/s}$ (almost completely deintercalated $2H\text{-TaS}_2$) gained continuously in intensity. The time evolution of the precession frequencies and the mole fractions derived from a nonlinear least-squares-fit analysis are illustrated in Fig. 3(b). With regard to the following discussion we wish to emphasize

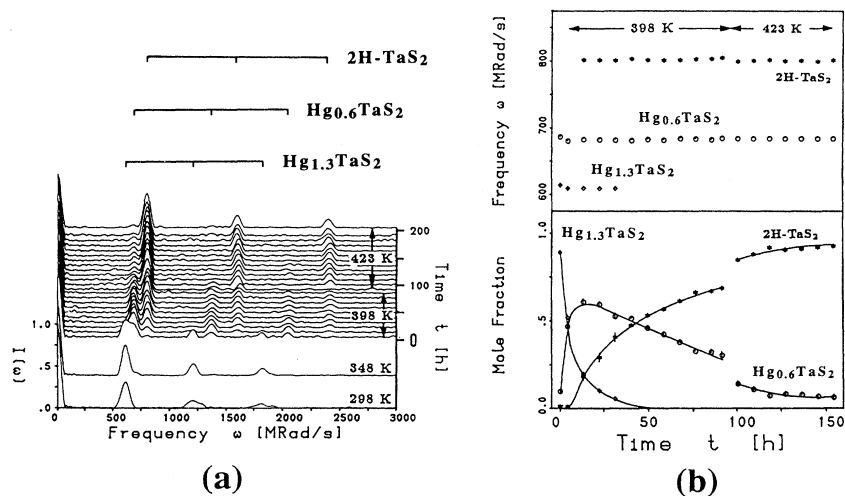


FIG. 3. (a) Stacked plot of Fourier-transformed TDPAC spectra recorded during the thermal deintercalation of Hg. (b) Temporal evolution of precession frequencies and mole fractions determined by a least-squares-fit analysis. Upon deintercalation at slightly elevated temperatures, the precession frequencies characteristic for a second-stage or random stage compound and residual $2H\text{-TaS}_2$ showed up.

the following items.

(1) Upon thermal Hg deintercalation, we observed the same frequency components as during the intercalation process. The slightly lower frequency values are due to a linear variation of the precession frequencies with temperature.

(2) As during intercalation, the precession frequencies of all three phases were constant throughout the entire deintercalation process.

(3) The time evolution of the mole fractions is, compared to the *in situ* investigation of the mercuration process, more or less time reversed, thus emphasizing the complete reversibility of the intercalation process.

(4) In combination with a strong temperature gradient, complete deintercalation can be obtained already at slightly elevated temperatures.

On the other side, it is possible to stabilize all three Hg intercalates to fairly high temperatures, if only the confining volume and the temperature gradients are small enough. E.g., sealed inside a tiny tube together with some excess mercury, the stage-1 Hg intercalates remained stable even at 521 K. In contrast to the previous experiment neither the NQI signal of the second-stage phase nor that of residual $2H$ -TaS₂ could be detected. Obviously, these observations outline the delicate free-energy balance between intercalated and elemental mercury.

3. Temperature evolution of the NQI

The precession frequencies of all three Hg intercalates decreased linearly between 13 and 521 K, as shown in Fig. 4(a) for β -Hg_xTaS₂. Such a linear frequency variation is quite common for TMD compounds and has been related to the two dimensionality of these materials.³⁶

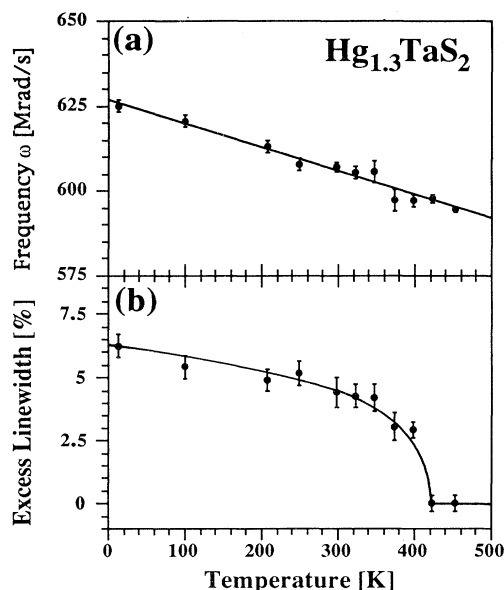


FIG. 4. The precession frequency and excess linewidth of the ¹⁸¹Ta NQI of β -Hg_xTaS₂ versus temperature. In order to avoid Hg deintercalation, the β -Hg_xTaS₂ has been sealed inside a tiny glass tube together with some Hg excess.

Note, that in agreement with our stage-2 interpretation, the frequency variation of the intermediate phase was found to lie between those of the stage-1 compounds and that of pristine $2H$ -TaS₂ (Table I). For α -Hg_xTaS₂ and the second-stage phase, the linewidth of the NQI signal remained instrumental throughout the whole temperature range. In contrast to this, β -Hg_xTaS₂ samples exhibited a sudden drop of the excess linewidth at an onset temperature of about 410 K [Fig. 4(b)]. Above this temperature, the linewidth of the NQI signal was found to be instrumental. The sudden decrease at 410 K could be related to a melting of the Hg sublattice (solid-liquid phase transition). In this case, the inequivalence between the different Ta sites would be wiped out by the strongly enhanced mobility of the intercalated Hg atoms (motional narrowing). However, there is a second possibility. Since the only difference between the NQI signals of β -Hg_xTaS₂ and α -Hg_xTaS₂ is the linewidth, the sudden decrease of the excess linewidth may also be related to a reversible transition from β -Hg_xTaS₂ to α -Hg_xTaS₂. The occurrence of such a phase transition involves necessarily a reversible intercalation/deintercalation of Hg, which is not unlikely, since the β -Hg_xTaS₂ samples have been stored in contact with a large amount of Hg excess.

4. Structural properties α -Hg_xTaS₂ ($2H$)

Pure single phase α -Hg_xTaS₂ samples were obtained at 473 K via the thermal deintercalation of β -Hg_xTaS₂, using the natural temperature gradient of a horizontal oven. A period of one day was usually sufficient to condense all the excess Hg at the colder end of the glass ampoule (~10 cm long). Weight measurements of the starting compounds and the recovered Hg excess revealed a non-stoichiometric Hg uptake of $x \sim 1.12(3)$. Essentially, the same result was obtained by the determination of the weight loss (TGA) of α -Hg_xTaS₂ samples during a complete deintercalation cycle.³⁵

A typical XPD diagram of the black metallic α phase is shown in Fig. 5 (top) and a d spacing list is given in Table II. The XPD reflections fall into two subsets, which we attribute to the expanded TaS₂ host lattice and a Hg sublattice, respectively. The TaS₂ subset of reflections can be indexed with a C-centered orthorhombic Bravais lattice [$a = 5.765(1)$ Å, $b = 3.309(1)$ Å, and $c = 17.842(1)$ Å]. However, there is no simple commensurate superstructure that would also explain the distances observed for the Hg sublattice.

A complete integer indexation of the whole diagram is nevertheless possible with the (3+1)-dimensional vector expression $\vec{M} = h\vec{a}^* + k\vec{b}^* + l\vec{c}^* + m\vec{b}_{\text{Hg}}^*$ (Table II), showing that the TaS₂ and Hg sublattices share two commensurate axes (a and c), but are incommensurate along the b axis [$b_{\text{Hg}} = 2.782(1)$ Å]. A similar indexation has been used to describe the composite crystal structure of Hg_{1.24}TiS₂ to which α -Hg_xTaS₂ is comparable in many respect.

(1) The increase of the c parameter of the TaS₂ host lattice from 12.097 to 17.842 Å corresponds to an expansion

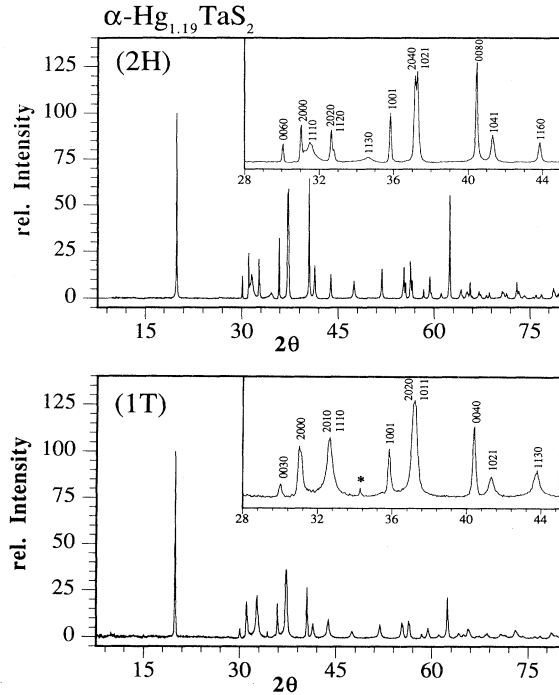


FIG. 5. X-ray powder-diffraction diagrams of $\alpha\text{-Hg}_x\text{TaS}_2$ prepared from $2H\text{-TaS}_2$ (top) and $1T\text{-TaS}_2$ (bottom), respectively. The indexing shown in the insets is based on orthorhombic sublattices and the vector expression given in Table II. Parasite reflections due to the INEL diffractometer are marked by a (*).

TABLE II. X-ray powder-diffraction data for $\alpha\text{-Hg}_{1.19}\text{TaS}_2$ ($2H$). The given d spacings and reflection intensities have been obtained in a full pattern matching mode by the MPROF program chain (Ref. 50). The lattice distances are related to the TaS_2 and Hg sublattice parameters given in Table III by the vector expression $H=ha^*+kb^*+lc^*+mb_{\text{Hg}}^*$. The quoted reflection intensities may differ from powder data, due to a high absorption coefficient and preferred orientation.

h	k	l	m	d_{obs}	I_{obs}	h	k	l	m	d_{obs}	I_{obs}
0	0	4	0	4.4492	100	1	1	6	0	2.0630	17
0	0	6	0	2.9685	7	1	0	6	1	1.9141	21
2	0	0	0	2.8779	18	1	1	7	0	1.9039	4
1	1	0	0	2.8653	6	2	0	8	0	1.7622	17
2	0	1	0	2.8413	5	1	1	8	0	1.7594	6
1	1	1	0	2.8291	40	1	0	8	1	1.6646	6
2	0	2	0	2.7388	19	3	1	0	0	1.6604	19
1	1	2	0	2.7283	15	0	2	0	0	1.6533	2
2	0	3	0	2.5903	5	3	1	1	0	1.6535	7
1	1	3	0	2.5809	13	3	1	2	0	1.6325	9
1	0	0	1	2.5022	30	2	0	9	0	1.6322	14
1	0	1	1	2.4781	2	1	1	9	0	1.6298	1
2	0	4	0	2.4182	48	0	2	2	0	1.6256	12
1	1	4	0	2.4107	7	3	0	0	1	1.5802	9
1	0	2	1	2.4094	63	3	1	4	0	1.5561	13
2	0	5	0	2.2399	1	3	0	2	1	1.5559	3
1	1	5	0	2.2340	4	1	0	9	1	1.5535	1
0	0	8	0	2.2277	67	0	2	4	0	1.5502	3
1	0	4	1	2.1822	33	3	0	4	1	1.4893	1

of the vdW gap of $\Delta c/2=2.873 \text{ \AA}$, which is about the vdW diameter of a Hg atom. A similar value of 2.962 \AA has been reported for $\text{Hg}_{1.24}\text{TiS}_2$.¹⁶

(2) Electron-diffraction photographs of the $(hk0)$ plane of thin $\alpha\text{-Hg}_x\text{TaS}_2$ single crystals recorded in transmission exhibited essentially the same diffraction pattern as previously observed for $\text{Hg}_{1.24}\text{TiS}_2$.^{16,17,37} The reflection positions on the photographs were found to be consistent with the $(3+1)D$ -vector expression and the lattice parameters given above.³⁷ Moreover, the diffraction photographs exhibit an angle of about 4° between the $[110]$ layerlines of the TaS_2 and the Hg sublattice. The observation of such an angle is quite characteristic for a $(3+1)D$ composite crystal structure and easily explained by the misfit of the two b sublattice parameters: $\varphi=\arctan(a/b_{\text{Hg}})-\arctan(a/b_{\text{TaS}_2})=4.09^\circ$.¹⁶

(3) The shortest distance between two neighboring Hg atoms in $\alpha\text{-Hg}_x\text{TaS}_2$ is found along the b axis and given by the b parameter of the Hg sublattice ($b_{\text{Hg}}=2.782 \text{ \AA}$). Similar Hg-Hg distances have been reported for many Hg compounds containing polymetallic Hg cations [e.g., Hg_2Cl_2 , $\text{Hg}_4(\text{AsF}_6)_2$, $\text{Hg}_{2.94}\text{AsF}_6$, and $\text{Hg}_{1.24}\text{TiS}_2$] and are characteristic for the formation of chainlike Hg-Hg metal bonds.^{16,22,38-40}

(4) Typical for $\alpha\text{-Hg}_x\text{TaS}_2$ is, furthermore, the occurrence of an orthorhombic distortion, which breaks the hexagonal symmetry of the TaS_2 slabs. The loss of the threefold rotation axis within the TaS_2 host slabs leads *inter alia* to a splitting of the normally degenerate (2020) and (1120) reflections (Fig. 5 top, inset). The orthorhombic distortion results mainly from a unidirectional stretching of the TaS_2 slabs along the pseudohexagonal a axis. Compared to pristine $2H\text{-TaS}_2$ the a parameter of $\alpha\text{-Hg}_x\text{TaS}_2$ is found to be larger by 0.026 \AA , whereas the b parameter has about the same value. A similar behavior has been reported for $\text{Hg}_{1.24}\text{TiS}_2$ and was explained by a repulsive interaction between neighboring Hg metal chains.¹⁶

(5) As for pristine $2H\text{-TaS}_2$ a doubling of the c parameter is required by the occurrence of additional reflections at lattice distances of 2.8291 and 2.5809 \AA attributed to the (1110) and the (1130) reflection, respectively (Fig. 5, top, inset). However, these additional reflections are peculiar for two reasons. First, the linewidth of the additional reflections is rather large compared to the rest, indicating a fairly high level of stacking faults that somehow must be related to the doubling of the unit cell. Second, the relative intensities of these reflections are unusually high compared to pristine $2H\text{-TaS}_2$. Since in the case of $2H\text{-TaS}_2$, only the sulfur sublattice contributes to the additional reflections, this observation implies a glide shift in either the Ta or the Hg sublattice. It is interesting to note that the mercuration of TiS_2 also causes a reversible shear transformation of the TiS_2 host layers.¹⁶ By this shear transformation, trigonal-prismatic sulfur channels are created in which the incommensurate Hg sublattice is embedded.

$\beta\text{-Hg}_x\text{TaS}_2$ ($2H$). The reaction of $2H\text{-TaS}_2$ with Hg in excess ($x > 1.3$) results in a homogeneous, copper-colored product called $\beta\text{-Hg}_x\text{TaS}_2$, for which TGA and

differential scanning calorimetry (DSC) studies indicated a Hg uptake of $x \sim 1.3(1)$.³⁵ A typical XPD pattern of this phase is shown in Fig. 6 (top).

With regard to the linewidth, the XPD reflections fall into two subsets which we again attribute to the TaS₂ (sharp reflections) and the Hg sublattice (broad reflections), respectively. The TaS₂ sublattice reflections can be indexed with a hexagonal Bravais lattice [$a_h = 3.317(1)$ Å, $c_h = 18.052(3)$ Å]. Compared to pristine 2H-TaS₂, this corresponds to a slight increase of the a parameter ($\Delta a \sim 0.003$ Å) and a vdW gap expansion of $\Delta c/2 = 2.98$ Å along the c axis, which is about the vdW diameter of elemental mercury. The doubling of the c parameter is required by the observation of a weak additional reflection next to the (100) reflection (Fig. 6, top, inset).

For the Hg sublattice the situation is less clear. Based on the XPD reflections positions, as well as on TEM electron diffraction photographs³⁷ of the $(hk0)$ plane, a hexagonal Hg layer [$a_{\text{Hg}} = 2.902(3)$ Å] has been proposed, which is rotated by 30° against the TaS₂ host lattice. Such a Hg arrangement would be quite close to commensurability and in the first approximation, one may indeed consider the TaS₂ host lattice as a centered 2×2 superstructure formed upon the hexagonal close-packed Hg layers. However, the XPD diagrams clearly point out the incom-

mensurability between the two sublattices. Moreover, the (100) Hg sublattice reflection exhibited a characteristic shoulder in all recorded XPD diagrams, which is neither explained by the assumption of hexagonal closed-packed Hg layers nor a domain wall model (discommensuration model). According to the latter model, which has been successfully applied to alkali-metal graphite intercalation compounds,^{41,42} discontinuous phase shifts within the Hg sublattice would create a periodic arrangement of commensurate Hg domains.

B. Mercury Intercalation into 1T-TaS₂

For the *in situ* investigations of the intercalation process, we sealed small 1T-TaS₂ crystals (sieve fraction: $315 < d < 500$ μm) in a glass ampoule together with a large excess of Hg. The sample was constantly stirred in order to ensure a good contact with the liquid Hg. Despite a prolonged waiting time of more than a fortnight all TDPAC spectra recorded at room temperature were found to be identical to that of pristine 1T-TaS₂ [Fig. 7(a), bottom spectrum].

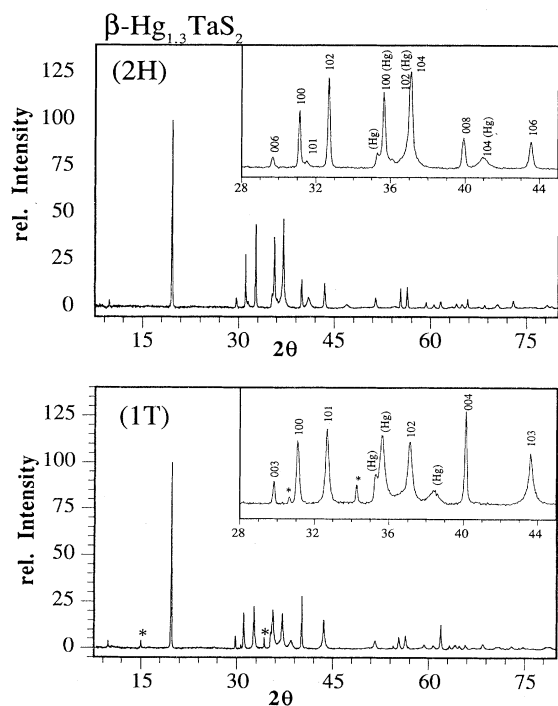


FIG. 6. X-ray powder diffraction diagram of $\beta\text{-Hg}_x\text{TaS}_2$ prepared from 2H-TaS₂ (top) and 1T-TaS₂ (bottom), respectively. The indexation shown in the insets is based on the hexagonal lattice as summarized in Table III. Reflections attributed to the Hg sublattice are indicated by the letters (Hg). Parasite reflections due to unreacted 1T-TaS₂ and the INEL diffractometer are marked by a (*).

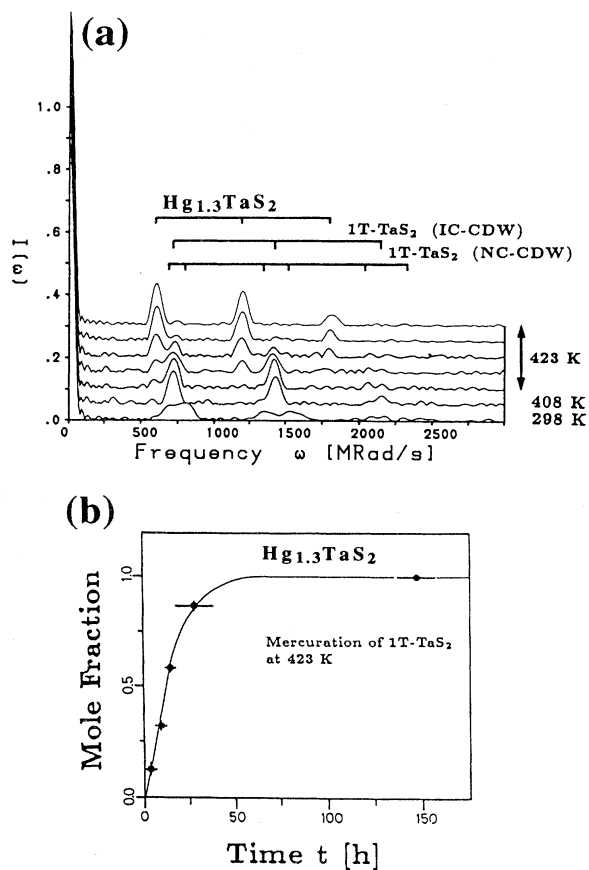


FIG. 7. Mercury intercalation into 1T-TaS₂: (top) Stacked plot of Fourier transformed TDPAC spectra showing the usual CDW phase transition at 353 K and the onset of Hg intercalation at 423 K; (bottom) time evolution of the mole fraction of $\beta\text{-Hg}_x\text{TaS}_2$.

Moreover, upon heating to 408 K, we obtained the same TDPAC spectra as we previously did for pristine $1T\text{-TaS}_2$: Below 353 K, the NQI signal is split into two fundamental frequency components, due to the nearly commensurate CDW present in pristine $1T\text{-TaS}_2$. At 353 K, a CDW phase transition from the nearly commensurate state to an incommensurate state occurs and above this temperature, the TDPAC spectra are composed of a single frequency component at 740 Mrad/s plus its harmonics [Fig. 7(a), second spectrum]. This phase transition is characteristic for high-quality $1T\text{-TaS}_2$ and, as a rule, easily suppressed or modified upon intercalation or the introduction of defects (e.g., by radiation damage or doping).⁴³ Hence, the observation of this CDW phase transition is a stringent criterion that Hg does not intercalate into $1T\text{-TaS}_2$, even at slightly elevated temperatures.

To trigger the reaction, a temperature of about 423 K was necessary. At this temperature, a frequency component appeared at $\omega'_1 \sim 609$ Mrad/s, while that of the pristine $1T\text{-TaS}_2$ vanished [Fig. 7(a)]. The intercalation reaction was then finished within two days [Fig. 7(b)] yielding a homogeneous, reddish colored product, which we termed $\beta\text{-Hg}_x\text{TaS}_2$ ($1T$).

As is implied by the choice of the name, there is a close relationship between the Hg intercalates derived from $2H\text{-TaS}_2$ and $1T\text{-TaS}_2$, respectively. In both cases, the obtained Hg intercalates were superstoichiometric with respect to their Hg uptakes ($x \sim 1.3$) and exhibited a typical reddish luster. The TDPAC spectra of both products were found to be identical and with decreasing temperature their NQI signals varied in the same way (Table I). Moreover, the XPD diagrams of $\beta\text{-Hg}_x\text{TaS}_2$ ($1T$) exhibited, apart from some details, essentially the same features as the corresponding $2H\text{-TaS}_2$ intercalation compound (Fig. 6, bottom). In both cases, the hexagonal TaS_2 host lattice had an a parameter of $3.318(1)$ Å, which is quite typical for $2H\text{-TaS}_2$ intercalates, but surprisingly small for a $1T\text{-TaS}_2$ intercalation compound. The observation of the same a parameter value for both products strongly suggests that the mercuration of $1T\text{-TaS}_2$ is connected with an irreversible change of the Ta coordination from octahedral to trigonal prismatic. Further evidence for such a Ta-coordination change comes from the fact that Hg deintercalation of $\beta\text{-Hg}_x\text{TaS}_2$ ($1T$) at 433 K yielded exactly the same results as for the corresponding $2H\text{-TaS}_2$ intercalation compound: upon deintercalation, we obtained the formation of a black-metallic phase termed $\alpha\text{-$

Hg_xTaS_2 ($1T$), a second-stage compound, and the residual host material, whose precession frequency ($\omega_1 \sim 818$ Mrad/s) and XPD diagram were characteristic for $2H\text{-TaS}_2$.

Although the Hg intercalates of $1T\text{-TaS}_2$ and $2H\text{-TaS}_2$ are, in general, closely related, their XPD diagrams exhibit some characteristic differences (Figs. 5 and 6).

$\alpha\text{-Hg}_x\text{TaS}_2$ ($1T$). As for the corresponding $2H\text{-TaS}_2$ intercalation compound, the electron-diffraction photographs of the $(hk0)$ plane,³⁷ as well as rotating crystal photographs recorded on a Weissenberg camera proved the formation of incommensurate Hg metal chains in the vdW gap (Table III). However, the indexation of the XPD diagram does not require a doubling of the c parameter (Fig. 5). The fairly intense extra reflections observed for $\alpha\text{-Hg}_x\text{TaS}_2$ ($2H$) are absent in the case of $\alpha\text{-Hg}_x\text{TaS}_2$ ($1T$). The c parameter is found to be slightly smaller than in $\alpha\text{-Hg}_x\text{TaS}_2$ ($2H$), $c = 8.910(1)$ Å, and the monoclinic distortion within the TaS_2 slabs is less pronounced as indicated by the b/a ratio (Table III). Together with the considerable deterioration of the crystal quality during the mercuration process, this results in a significant broadening of the XPD reflections.

$\beta\text{Hg}_x\text{TaS}_2$ ($1T$). With respect to the TaS_2 sublattice, the differences in the XPD diagrams are limited to a slightly smaller c parameter, $c = 8.977(1)$, and the absence of the additional reflection which requires a doubling of the c parameter in the case of $\beta\text{-Hg}_x\text{TaS}_2$ ($2H$). However, there are some major differences with respect to the Hg sublattice. Although the shortest Hg sublattice distances, represented by the (100) reflection and its characteristic shoulder, are common to both phases, there are many reflections which are present in one phase but absent in the other. The origin of these differences is not yet clear, but they seem to be related to a different Hg arrangement within the vdW gap.

IV. DISCUSSION

A. Ta coordination change

Mercury intercalation into $1T\text{-TaS}_2$ requires, in contrast to the isostructural $1T\text{-TiS}_2$ and the $2H\text{-TaS}_2$ polymorph, an elevated reaction temperature of about 423 K. The resulting intercalation product is found to be closely related to the corresponding $2H\text{-TaS}_2$ intercalates. The nearly identical structural and physical properties, and the fact that upon a complete intercalation/

TABLE III. Crystallographic data for $\alpha\text{-Hg}_{1.19}\text{TaS}_2$ and $\beta\text{-Hg}_{1.3}\text{TaS}_2$. In the case of $\beta\text{-Hg}_x\text{TaS}_2$ ($1T$), it was not possible to index the few Hg sublattice reflections with a hexagonal lattice.

Compound	Crystal system	Lattice parameters
$\alpha\text{-Hg}_x\text{TaS}_2$ ($2H$)	orthorhombic	$a = 5.765(1)$ Å, $b = 3.309(1)$ Å, $c = 17.842(1)$ Å, $b_{\text{Hg}} = 2.782(1)$ Å, $b/a = 1.742$
$\alpha\text{-Hg}_x\text{TaS}_2$ ($1T$)	orthorhombic	$a = 5.757(2)$ Å, $b = 3.318(1)$ Å, $c = 8.910(1)$ Å, $b_{\text{Hg}} = 2.781(1)$ Å, $b/a = 1.735$
$\beta\text{-Hg}_x\text{TaS}_2$ ($2H$)	hexagonal	$a = 3.317(1)$ Å, $c = 18.052(3)$ Å, $a_{\text{Hg}} = 2.902(3)$ Å
$\beta\text{-Hg}_x\text{TaS}_2$ ($1T$)	hexagonal	$a = 3.318(1)$ Å, $c = 8.977(1)$ Å

deintercalation cycle $2H\text{-TaS}_2$ is obtained as residual compound, indeed suggest that the mercuration of $1T\text{-TaS}_2$ is connected with an irreversible change of the Ta coordination from octahedral to trigonal prismatic. A similar "soft chemistry induced" coordination change within the covalently bound TaS_2 layers has been observed upon the chemical lithiation of $1T\text{-TaS}_2$ and the ambient temperature intercalation of sodium via a sodium amalgam.⁷ The minor structural differences between the Hg intercalates prepared from $2H\text{-TaS}_2$ and $1T\text{-TaS}_2$ are probably due to a different stacking sequence of the TaS_2 lamellas and in the case of $\beta\text{-Hg}_x\text{TaS}_2$ to a different Hg arrangement within the vdW gap. The occurrence of these differences may be related to the fact that after intercalation, the full thermal equilibrium has not yet been obtained.

B. Compositions

Upon Hg intercalation into TaS_2 or thermal deintercalation, we observed the subsequent evolution of three distinct phases (a random stage or second-stage phase, $\alpha\text{-Hg}_x\text{TaS}_2$, and $\beta\text{-Hg}_x\text{TaS}_2$), each of which is characterized by a well-defined precession frequency. Unlike for many other TaS_2 intercalation reactions, these precession frequencies were found to be constant throughout the whole intercalation/deintercalation process independent of the reaction kinetics. This suggests that certain in-plane Hg packing densities are energetically favored. A similar observation has been reported for $\text{Hg}_{1.24}\text{TiS}_2$.⁴⁴ Here, dynamic HRTEM revealed that the thermal deintercalation of Hg proceeds by the subsequent deintercalation of entire guest layers rather than by the dilution of the in-plane Hg packing density.

However, compared to the latter, the Hg_xTaS_2 system is by far more complicated. Besides the black metallic $\alpha\text{-Hg}_x\text{TaS}_2$ and the corresponding random stage or second-stage compound a copper-colored phase ($\beta\text{-Hg}_x\text{TaS}_2$) is formed in the presence of excess Hg. As for $\alpha\text{-Hg}_x\text{TaS}_2$, this phase is "superstoichiometric" in its Hg uptake, e.g., there are more Hg atoms in a guest monolayer than there are specific crystallographic sites offered by the TaS_2 host structure. Its stoichiometry is close to $x \sim 1.3$, as can be judged from the available crystallographic data obtained by TEM and XPD.³⁷ This estimate is in perfect agreement with recent TGA and DSC studies.³⁵

Based on the diffraction data, the ideal composition of $\alpha\text{-Hg}_x\text{TaS}_2$ is, as will be discussed later on, $x = 1.19$ in perfect agreement with our TDPAC estimate. The somewhat lower values obtained by TGA (Ref. 35), ($x \sim 1.1$) are probably related to vacancies within the Hg sublattice, which may be an intrinsic feature of the $\alpha\text{-Hg}_x\text{TaS}_2$ crystal structure.

For lower formal Hg compositions, the TDPAC data suggest the formation of a second-stage and/or a random stage compound derived from $\alpha\text{-Hg}_x\text{TaS}_2$. Because of the very local nature of the information provided by TDPAC measurements it is, in general, impossible to distinguish between different staging arrangements. However, the fact that the mole fraction of the intermediate phase

reached more than 56% during thermal deintercalation, indicates at least the existence of a highly disordered second-stage phase. This suggestion has been confirmed by x-ray powder diffraction.⁴⁵ For compositions lower than $x \sim 1.1$, the XPD diagrams exhibited an asymmetrical broadening of the $(00l)$ reflections related to the increasing number of staging defects and around $x \sim 0.6$, the $(00l)$ reflections of a disordered second-stage compound have been observed.

In addition to the three phases stated above, a $\text{Hg}_{1.0}\text{TaS}_2$ compound has been described in earlier publications.^{15,46} However, the comparison of the d -spacing list published by Di Salvo *et al.* for $\text{Hg}_{1.0}\text{TaS}_2$ with that given in Table II shows that the former Hg intercalation compound can be identified as $\alpha\text{-Hg}_x\text{TaS}_2$.

C. Crystal structures

$\alpha\text{Hg}_x\text{TaS}_2$. Based on our experimental observations and the close relationship between $\alpha\text{-Hg}_x\text{TaS}_2$ and $\text{Hg}_{1.24}\text{TiS}_2$, the following structure model can be derived [Fig. 8(a)]. As for $\text{Hg}_{1.24}\text{TiS}_2$, the α phase adopts an unusual $(3+1)D$ -composite crystal structure, which can be described as two interpenetrating C-centered orthorhombic sublattices formed by the TaS_2 host layers and the Hg guest layers, respectively. These sublattices share

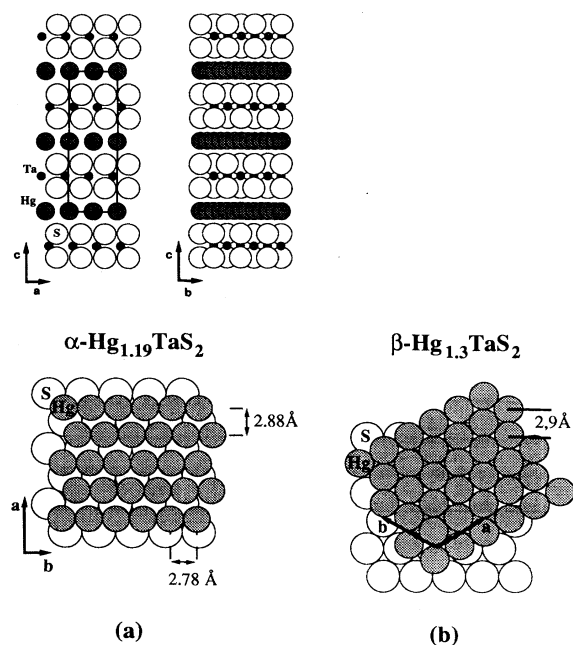


FIG. 8. (a) Schematic illustration of the $\alpha\text{-Hg}_x\text{TaS}_2$ crystal structure: (top left) a projection along the b axis showing the interlayer structure viewed parallel to the Hg chains; (top right) a projection along the a axis showing the interlayer structure viewed perpendicular to the chains; (bottom) a projection perpendicular to the layers showing the relative intralayer arrangement of the Hg atoms with respect to a neighboring S layer. (b) Schematic illustration of the relative intralayer arrangement of Hg atoms in $\beta\text{-Hg}_x\text{TaS}_2$.

two commensurate axes (**a** and **c**), but are incommensurate along the **b** axis. Alternatively, the Hg sublattice may be considered as an ordered array of infinite Hg chains, whose periodicity is incommensurate to that of the TaS₂ host. However, the registry of these Hg chains is commensurate with respect to the **a*** and **c*** axes of the TaS₂ sublattice, where at least the commensurability along **c*** is evident since the compact host and guest layers cannot penetrate each other. Although a complete Rietveld structure analysis of the available XPD data failed due to the problems related to a high absorption coefficient ($\mu_a \sim 170 \text{ cm}^{-1}$) and preferred orientation, it seems likely that in analogy to Hg_{1.24}TiS₂, the incommensurate Hg chains are embedded into trigonal-prismatic sulfur channels as is depicted in Fig. 8(a). Starting from 2*H*-TaS₂, the creation of these sulfur channels requires a glide shift of $\pm 1/3a$ for every second TaS₂ slab. Note, that in agreement with our experimental observations, it is now the Ta sublattice that imposes the doubling of the *c* parameter. In the case of 1*T*-TaS₂, the intercalation of Hg is probably connected with an irreversible shear transformation within the sulfur layers, which could at the same time change the coordination of the Ta atoms and create the trigonal-prismatic sulfur channels in the vdW gap. Since such a shear transformation leaves the Ta sublattice invariant, the α -Hg_{*x*}TaS₂ (1*T*) crystal structure would not require a doubling of the *c* parameter, which is consistent with the recorded XPD diagrams. As for Hg_{1.24}TiS₂, the intralayer arrangement of Hg chains bears a strong resemblance to the (110) planes of β -Hg, which exhibit similar intrachain and interchain Hg-Hg distances of 2.782 and 3.158 Å, respectively.²³

The incommensurability between the two sublattices implies an infinite number of different Ta sites. Hence, one would expect to observe a frequency distribution rather than a single Ta site as we did for α -Hg_{*x*}TaS₂. However, any modulation of the Hg and TaS₂ sublattices, due to local guest-host interactions, will render the different sites more equivalent and thus difficult to resolve experimentally. The occurrence of such modulations has been proved directly in the case of Hg_{1.24}TiS₂.¹⁷ HRTEM images taken along the *c* axis of thin Hg_{1.24}TiS₂ platelets exhibited a slight *a* axis modulation (~ 0.2 Å) of the dark-contrast spots, due to a transversal modulation of the linear Hg metal chains. It is interesting to note that despite the incommensurability between the Hg guest and the TiS₂ host sublattice, the investigation of the ^{199m}Hg NQI in Hg_{1.24}TiS₂ revealed a single Hg site, only.⁴⁷ The EFG at this unique Hg site exhibited, nevertheless, a strong deviation from axial symmetry ($\eta = 0.41$) in direct support of a chainlike Hg arrangement.

β -Hg_{*x*}TaS₂. In contrast to Hg_{*x*}TiS₂ intercalates, which exhibit the chainlike Hg arrangement only, a second possibility is realized in β -Hg_{*x*}TaS₂. Here, the intercalated Hg forms approximately a hexagonal close-packed Hg layer, which is sandwiched between the neighboring TaS₂ layers as depicted in Fig. 8(b). Each Hg atom has on the average six nearest neighbors with a Hg-Hg bond length of 2.91 Å. This description has some striking analogies. Besides the chainlike Hg arrangement usually realized in

Hg₃₋₈MF₆ compounds (*M* = As, Sb, Ta, Nb), a second structure has been reported for Hg₃MF₆ (*M* = Nb, Ta).²² In the latter compounds, hexagonal close-packed Hg sheets with a Hg-Hg distance of 2.90 Å are separated by close-packed layers of MF₆ octahedrons.

In β -Hg_{*x*}TaS₂, the TaS₂ sublattice can be considered as a 2×2 superstructure formed upon hexagonal close-packed Hg layers to a good approximation. If the origin of the two sublattices coincides, this would result in two inequivalent Ta sites with a population of 2:1. Other phasings would either lead to the same result or give three inequivalent sites with equal population. In any case, the significant line broadening of the β -Hg_{*x*}TaS₂ NQI signal could be due to an unresolved splitting of the EFG at the different Ta sites. This would also explain the slight deviation from axial symmetry ($\eta \sim 0.1$) that has been observed for β -Hg_{*x*}TaS₂ samples typically. However, the line broadening as well as the deviation from axial symmetry could also be related to the incommensurability of the Hg sublattice.

D. Guest-host and guest-guest electronic interactions

For 2*H*-TaS₂ intercalation compounds, an empirical relationship between the precession frequency ω (in Mrad/s) and the charge transfer *n* has been established by numerous TDPAC studies,^{48,49}

$$\omega \sim 820 - 745n + 293n^2. \quad (9)$$

This relation turned out to be quite insensitive to the nature of the guest species and the specific sites occupied in the vdW gap. Its application yields a "charge-transfer" estimate of $n \sim 0.18 e^-/\text{Ta}$ for the second-stage phase and of $n \sim 0.32 e^-/\text{Ta}$ for α -Hg_{*x*}TaS₂ and β -Hg_{*x*}TaS₂, respectively. A similar estimate ($n \sim 0.25 e^-/\text{Ti}$) has been quoted for Hg_{1.24}TiS₂ based on the investigation of the magnetic susceptibility.¹³ These estimates agree well with the formal $+1/3$ oxidation state found in the structurally related Hg₃₋₈MF₆ compounds.^{21,22} However, in disagreement to our TDPAC studies, which favor an ionic description of the Hg-S interaction, ion exchange and redox intercalation studies on Hg_{*x*}TiS₂ suggested a very low level of ionic charge transfer, but allow the possibility of a weak covalent electron exchange.¹⁰ Essentially the same conclusion is obtained if one compares the interchain Hg-Hg distances in Hg_{1.24}TiS₂ and α -Hg_{*x*}TaS₂ to the Hg^{*n*+}-Hg^{*n*+} bond distances for compounds containing linear Hg chains with a known ionic value.¹⁶

Although the exact nature of the Hg-S interaction remains questionable, there is one important point that all methods agree upon: the interaction between the TDM host and the Hg guest atoms is found to be surprisingly weak, as suggested by the easy reversibility of the intercalation process and the small degree of charge transfer. On the other side, there is substantial Hg-Hg bonding between the intercalated Hg atoms. The Hg-Hg distances found in α -Hg_{*x*}TaS₂ (2.78 and 3.20 Å) and β -Hg_{*x*}TaS₂ (~ 2.91 Å) are comparable to the Hg-Hg bond lengths reported for β -Hg (2.88 and 3.18 Å) and α -Hg (2.993 Å). Note, that it is this unique combination of a

interaction with a comparatively weak guest-host interaction that largely accounts for the properties of Hg-TMDIC's.

V. CONCLUSIONS

By the combination of TDPAC and x-ray-diffraction techniques, we proved that Hg intercalation into TaS₂ results in the formation of three distinct phases (α -Hg_{1.19}TaS₂, β -Hg_{1.3}TaS₂, and a disordered second-stage phase Hg_{0.58}TaS₂ derived from α -Hg_xTaS₂). As in solid Hg itself, two possible Hg arrangements are realized in the TaS₂ vdW gap. These arrangements comprise an ordered array of incommensurate Hg chains in α -Hg_xTaS₂ and approximately hexagonal close-packed Hg guest layers in β -Hg_xTaS₂. Similar Hg arrangements and bond lengths have been observed in many other compounds that contain polymercury cations, but also in the Hg solid-state phase α -Hg and β -Hg, respectively. Especially the latter analogy clearly indicates that the structural arrangement of the intercalated Hg atoms is largely governed by metallic Hg-Hg interactions. As a consequence each phase is characterized by a well-defined Hg packing density, which is intimately related to the specific type of Hg-Hg interaction. Deviations from the ideal stoichiometry are typically due to the occurrence of defects, such as point defects (vacancies) within the incom-

mensurate Hg chains, a random staging of filled and empty host galleries, and compact guest islands within partially intercalated/deintercalated galleries (Dauman-Hérol model).

In addition to the fairly strong guest-guest interaction, there is only a weak interaction between the intercalated Hg and the TaS₂ host. The competition between these interactions results in unusual composite crystal structures. These structures can be considered as a mutual alignment of two (or more) subsystems, whose structural compositions are governed by different building principles. As in the case of Hg_{1.24}TiS₂, it seems likely that the guest-host interaction is related to a weak Hg-S bonding. Consistent with the local nature of the interaction, Hg-TMDIC's exhibit a large quantity of intrinsic stacking faults and upon partial deintercalation disordered second-stage or random stage compounds are formed only.

ACKNOWLEDGMENTS

It is a pleasure to thank Professor J. Rouxel, Professor G. M. Kalvius, and Professor K. Andres for their continuous interest and support. This work was supported by the EC program *Human Capital and Mobility* (PG) and the Bundesministerium für Bildung und Erziehung, Wissenschaft und Technologie. The reactor irradiations were kindly performed at the Forschungszentrum Jülich.

*On leave from Walter-Meißner Institut für Tieftemperaturforschung der Bayerischen Akademie der Wissenschaften, D-85748 Garching, FRG.

[†]Permanent address: Universität Leipzig, Fakultät für Physik und Geowissenschaften, D-04103 Leipzig, FRG.

¹J. Rouxel, in *Intercalated Layered Materials*, edited by F. Lévy (Reidel, Dordrecht, 1979), p. 201.

²G. V. Subba Rao and M. V. Schafer, in *Intercalated Layered Materials* (Ref. 1), p. 99.

³R. H. Friend and A. B. Yoffe, *Adv. Phys.* **36**, 1 (1989).

⁴R. M. A. Lieth and J. C. J. M. Terhell, in *Preparation and Crystal Growth of Materials with Layered Structures*, edited by R. M. Lieth (Reidel, Dordrecht, 1977), p. 141.

⁵J. A. Wilson, F. J. Di Salvo, and S. Mahajan, *Adv. Phys.* **24**, 117 (1975).

⁶M. A. Py and R. R. Haering, *Can. J. Phys.* **61**, 76 (1983).

⁷P. Ganal, W. Olberding, T. Butz, and G. Ouvrard, *Solid State Ionics* **59**, 313 (1993).

⁸R. Brec, *Mater. Sci. Eng. B* **3**, 73 (1989).

⁹M. McKelvy, R. Sharma, E. Ong, G. Burr, and W. Glaunsinger, *Chem. Mater.* **3**, 783 (1991).

¹⁰E. W. Ong, M. J. McKelvy, G. Ouvrard, and W. S. Glaunsinger, *Chem. Mater.* **4**, 14 (1992).

¹¹P. Moreau and G. Ouvrard, in *Chemical Physics of Intercalation II*, Vol. 305 of *NATO Advanced Study Institute, Series B: Physics*, edited by P. Bernier, J. E. Fischer, S. Roth, and S. A. Solin (Plenum, New York, 1993), p. 351.

¹²P. Ganal, W. Olberding, T. Butz, and G. Ouvrard, in *Chemical Physics of Intercalation II* (Ref. 11), p. 383.

¹³P. Moreau, P. Ganal, and G. Ouvrard, *Mol. Cryst. Liq. Cryst.* **244**, 325 (1994).

¹⁴T. Tracey, P. S. Gentile, and J. T. Budnick (unpublished).

¹⁵F. J. Di Salvo, G. W. Hull, Jr., L. H. Schwartz, J. M. Voorhoeve, and J. V. Waszczak, *J. Chem. Phys.* **59**, 1922 (1973).

¹⁶P. Ganal, P. Moreau, G. Ouvrard, M. Sidorov, M. McKelvy, and W. Glaunsinger, *Chem. Mater.* **7**, 1132 (1995).

¹⁷M. Sidorov, M. McKelvy, R. Sharma, W. Glaunsinger, P. Ganal, P. Moreau, and G. Ouvrard, *Chem. Mater.* **7**, 1140 (1995).

¹⁸R. J. Gillespie and P. K. Ummat, *J. Chem. Soc. Chem. Commun.* **1971**, 1168.

¹⁹A. J. Schultz, J. M. Williams, N. D. Miro, A. G. MacDiarmid, and A. J. Heeger, *Inorg. Chem.* **17**, 646 (1978).

²⁰Z. Tun and I. D. Brown, *Acta. Crystallogr. Sec. B* **38**, 2321 (1982).

²¹I. D. Brown, R. J. Gillespie, K. R. Morgan, Z. Tun, and P. K. Ummat, *Inorg. Chem.* **23**, 4506 (1984).

²²I. D. Brown, W. R. Datars, R. J. Gillespie, K. R. Morgan, Z. Tun, and P. K. Ummat, *J. Solid State Chem.* **57**, 34 (1985).

²³M. Atoji, J. E. Schirber, and C. A. Swenson, *J. Chem. Phys.* **31**, 1628 (1959).

²⁴*Table of Isotopes*, edited by L. M. Lederer, J. M. Hollander, and I. Perlman (Wiley, New York, 1967).

²⁵H. Frauenfelder and R. M. Steffen, in *Alpha-, Beta-, Gamma-Ray Spectroscopy*, edited by K. Siegbahn (North-Holland, Amsterdam, 1965), Vol. 2, p. 997.

²⁶N. Buttler, Ph.D. thesis, Universität Bonn, Germany, 1970.

²⁷T. Butz, *Hyperfine Interact.* **52**, 189 (1989).

²⁸P. Ganal (unpublished).

²⁹R. M. Steffen and H. Frauenfelder, in *Perturbed Angular Correlations*, edited by E. Karlson, E. Matthias, and K. Siegbahn (North-Holland, Amsterdam, 1964), p. 3.

³⁰A. Lerf and T. Butz, *Angew. Chem.* **99**, 113 (1987).

- ³¹P. Deniard, M. Evain, J. M. Barbet, and R. Brec, *Mater. Sci. Forum* **79-82**, 363 (1991).
- ³²M. Evain, P. Deniard, A. Jouanneaux, and R. Brec, *J. Appl. Cryst.* **26**, 563 (1993).
- ³³T. Butz, S. Saibene, Th. Fraenzke, and M. Weber, *Nucl. Instrum. Method Phys. Res. Sect. A* **284**, 417 (1989).
- ³⁴P. Ganal, Ph.D. thesis, Technische Universität München, Germany, 1992.
- ³⁵P. Moreau, Ph.D. thesis, Université de Nantes, France, 1994.
- ³⁶D. R. Trogeson and F. Borsa, *Phys. Rev. Lett.* **37**, 956 (1976).
- ³⁷P. Moreau, P. Ganal, A. M. Marie, and G. Ouvrard, *Inorg. Chem.* (to be published).
- ³⁸G. Torsi, K. W. Fung, G. H. Begun, and G. Manatov, *Inorg. Chem.* **10**, 2285 (1975).
- ³⁹B. D. Cutforth, C. G. Davies, P. A. W. Dean, R. J. Gillespie, P. R. Ireland, and P. K. Ummat, *Inorg. Chem.* **12**, 1343 (1973).
- ⁴⁰B. D. Cutforth, R. J. Gillespie, P. R. Ireland, J. F. Sawyer, and P. K. Ummat, *Inorg. Chem.* **22**, 1344 (1983).
- ⁴¹A. R. Kortan, A. Erbil, R. J. Birgenau, and M. S. Dresselhaus, *Phys. Rev. Lett.* **49**, 1427 (1982).
- ⁴²Y. Yamada and I. Naiki, *J. Phys. Soc. Jpn.* **51**, 2174 (1982).
- ⁴³P. Ganal, T. Butz, W. Karle, K.-H. Speidel, and A. Lerf, *Hyperfine Interact.* **60**, 903 (1990).
- ⁴⁴M. McKelvy, M. Sidorov, A. Marie, R. Sharma, and W. Glaunsinger, *Chem. Mater.* **6**, 2233 (1994).
- ⁴⁵S. Lemaux (unpublished).
- ⁴⁶A. C. Gossard, F. J. Di Salvo, and H. Yasuoka, *Phys. Rev. B* **9**, 3965 (1974).
- ⁴⁷W. Tröger, T. Butz, and G. Ouvrard, *Hyperfine Interact.* **80**, 1149 (1993).
- ⁴⁸T. Butz and A. Lerf, *Rev. Chim. Min.* **19**, 496 (1982).
- ⁴⁹C. Ramos, A. Lerf, and T. Butz, *Hyperfine Interact.* **61**, 1209 (1990).
- ⁵⁰A. D. Murray and A. N. Fitch, *MPROF: a Multipattern Rietveld Refinement Program for Neutron, X-ray and Synchrotron Radiation* (SERC Daresbury Laboratory, Warrington, England, 1992).